

# RSC Advances



This is an *Accepted Manuscript*, which has been through the Royal Society of Chemistry peer review process and has been accepted for publication.

*Accepted Manuscripts* are published online shortly after acceptance, before technical editing, formatting and proof reading. Using this free service, authors can make their results available to the community, in citable form, before we publish the edited article. This *Accepted Manuscript* will be replaced by the edited, formatted and paginated article as soon as this is available.

You can find more information about *Accepted Manuscripts* in the [Information for Authors](#).

Please note that technical editing may introduce minor changes to the text and/or graphics, which may alter content. The journal's standard [Terms & Conditions](#) and the [Ethical guidelines](#) still apply. In no event shall the Royal Society of Chemistry be held responsible for any errors or omissions in this *Accepted Manuscript* or any consequences arising from the use of any information it contains.

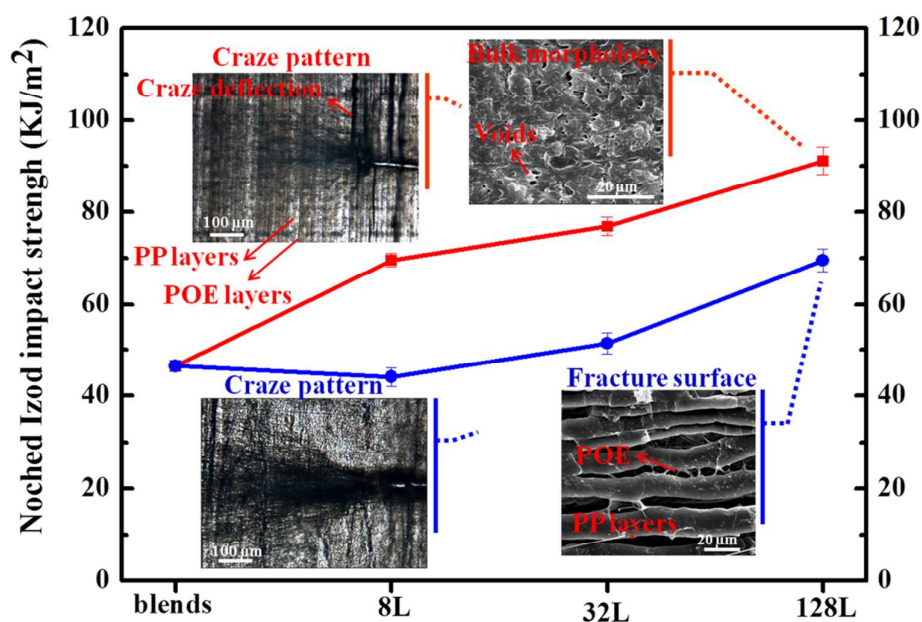
# Unique impact behavior and toughening mechanism of the polypropylene and poly(ethylene-co-octene) alternating multilayered blends with superior toughness

Chunhai Li, Shuo Yang, Jianfeng Wang, Jiwei Guo, Hong Wu\*, Shaoyun Guo\*

The State Key Laboratory of Polymer Materials Engineering, Polymer Research

Institute of Sichuan University, Chengdu 610065, China

## Graphical Abstract



In this study, the alternating multilayered PP/POE blends with different layers were successfully fabricated by the micro-co-extrusion. Compared with the conventional sea-island micro-structure, the unique alternating multilayered micro-structure of the multilayered blends has a great advantage in toughening PP. The notable improvement of toughness

in the alternating multilayered blends is ascribed to the synergetic effects of the interfaces delaminations, craze deflection, larger subcritical damage zone (stress whitening zone) and the combination of the voids and deformation during fracture process.

# Unique impact behavior and toughening mechanism of the polypropylene and poly(ethylene-co-octene) alternating multilayered blends with superior toughness

*Chunhai Li, Shuo Yang, Jianfeng Wang, Jiwei Guo, Hong Wu\*, Shaoyun Guo\**

*The State Key Laboratory of Polymer Materials Engineering, Polymer Research*

*Institute of Sichuan University, Chengdu 610065, China*

## ABSTRACT

In this study, a novel approach is proposed to toughen polypropylene (PP) significantly by fabricating PP and poly(ethylene-co-octene) (POE) into alternating multilayered blends instead of conventional blends. POM, SEM, Polarized-FTIR, DSC and XRD were performed to investigate and characterize the microstructure of the alternating multilayered and conventional blends. The crack-initiation term, impact fracture surface and bulk morphologies beneath the fracture surface are inspected to understand the differences in impact behaviors of the alternating multilayered blends and the conventional blends. The results show that the unique multilayered structure has a great advantage in toughening PP. The notable improvement of the toughness of the alternating multilayered blends is

---

\* To whom correspondence should be addresses. (Prof. Wu, Email: [wh@scu.edu.cn](mailto:wh@scu.edu.cn), Fax: 86-028-85466077)

\* To whom correspondence should be addresses. (Prof. Guo, Email: [sguo@scu.edu.cn](mailto:sguo@scu.edu.cn), Fax: 86-028-85405135)

ascribed to the synergetic effects of the interfaces delaminations, craze deflection, larger subcritical damage zone (stress whitening zone) and the combination of the voids and deformation during fracture process. Moreover, the alternating multilayered blends exhibit high toughness with a low POE content, thus this work also offers a new way to toughen materials without obvious sacrifice of the strength.

**Keywords:** Multilayered interfaces; PP; POE; Craze deflection; Toughening mechanism

## INTRODUCTION

Polypropylene (PP), one of the most widely used commodity plastics, has been the subject of intensive studies with the objective to improve its mechanical properties, especial impact toughness. One of the most effective methods is blending PP with elastomers [1]. Unfortunately, in such way, PP blends with high toughness usually accompany with obvious drops in the strength, and the cost also increases due to the high price of the elastomers. Therefore, how to balance the strength and the toughness of the PP/elastomers blends is highly desirable for many industrial applications. In general, the addition of rigid particles into polymers usually leads dramatic drops in fracture toughness, compared to their corresponding pristine polymers. Only a few studies have reported the enhancement of both the toughness and the strength [2~5]. However,

the extent of toughness enhancement, if at all, is not always significant. Thus, many studies [6~9] have been conducted on the polymer/elastomer/rigid filler ternary system. It has been found that the good dispersion of the rigid filler or elastomer makes a key role for achieving the best combination of mechanical properties. In order to achieve high impact toughness in the polymer/elastomer/rigid filler ternary system, the compatibilizers and surfactants are often used, which mean the tedious fabrication processes and the incorporation of costly steps. Besides, more or less drops in the flow-ability of the polymer melts always occur, resulting in the processing difficulty. Therefore, it's highly desirable for achieving the high toughness of the PP/elastomer composites without obvious sacrifice of the strength.

On the other hand, the design of the composites inspired by the hierarchical micro-structure, which was found in nature's load-bearing materials, is an efficient route to obtain the materials with unique combination of strength and toughness [10, 11]. Wood, spider silk, bone, tendon and nacre, such bio-composites are characterized by ordered structures combining large fractions of hard and reinforcing segments with a minor amounts of soft, energy-absorbing and lubricating biopolymer. Inspired by such biological architectures, many advanced technologies such as the electrical fields [12], tape-casting [13], layer-by-layer [14], and gel casting combined with hot-pressing [15, 16],

have been developed for preparing novel composites with superior mechanical properties, while these approaches are often limited to fabricate thin films and/or require multiple processing steps [17]. However, in past decades, multilayered micro-co-extrusion [18], which have been developed as a novel technology in polymer melt processing to tune the materials properties, such as the barrier [19], optical [20], electrical [21], especially mechanical properties [22~32].

Baer *et al.* [22~27] investigated the crazing behaviors of the co-extruded multilayered sheets of the polycarbonate (PC) and styrene-acrylonitrile copolymer (SAN) alternating layers. They found that a shift in the deformation mode from craze opening to the shear yielding as the individual layer was thin enough, which toughened the multilayered PC/SAN composites dramatically. Similarly, the brittle-to-ductile transition of the PS/SEPS multilayered films was also found when the thickness of the SEPS layer was thin enough [28~29]. Except the crazing behaviors under the quasi-static uniaxial tension, the PC/SAN and PC/PMMA multilayered sheets were also examined in dynamic ballistic test [27, 30]. With increasing the layer number, the multilayered sheets fractured with more profuse cracking, delaminations, and emergence of a circular impression, indicating that more impact energy was absorbed, and finally the projectile did not penetrate the specimens. Shen *et al.* [31] simulated the mechanical properties of the

PP/POE multilayered blends by equivalent box model and found that the yield strength of multilayered blends was higher than that of the conventional blends with the same POE content due to the high phase continuity of the multilayered blends. Herein, it can be concluded that combining two polymers with alternating multilayered architecture indeed endows the materials with excellent mechanical properties. However, one may note that all these excellent properties were dated from the sheets or films as the thickness of multilayered co-extrusion samples is usually lower than 1.5 mm. Because the polymers are viscoelastic, their toughness generally exhibit geometry and strain-rate dependence. Moreover, most materials are used as load-bearing bulk materials with different shapes and sizes. Consequently, it's necessary and significant to evaluate the toughness of multilayered materials in different test standards. In our previous work [32], we fabricated multilayered materials by alternating the PP and the PP/POE blend, which mean the alternating distribution of the POE particles in PP matrix, and then the multilayered sheets were hot-pressed into impact bars for Izod test. Most interestingly, compared with the random distribution of POE particles, the unique alternating distribution of POE particles endowed the materials with great enhancement of the toughness at  $-40^{\circ}\text{C}$ . As the damage prone to occurring at the interfaces, and a huge of interfaces are a great advantage in accumulating micro-cracks, delaminations and crack

deflection, all of which will toughen the materials obviously [33~35]. Therefore, we speculate that it should be more striking enhancement of the toughness for the PP/POE alternating multilayered blends, where the POE phase is distributed with a laminar morphology.

In this work, we attempt to imitate the micro-structures of nacre partly by introducing the alternating multilayered structure into PP toughening system, where higher fractions “stiff” PP layer and lower fractions “soft” POE layer alternate through multilayered micro-co-extrusion technology. The fracture behaviors of the alternating multilayered and conventional blends are investigated. The unique alternating multilayered micro-structure with PP layers and POE layers as well as large amounts of weak PP/POE interfaces will obviously toughen the multilayered blends without obvious drop in the strength.

## **2 EXPERIMENTAL**

### **2.1 Materials**

The PP is 1300 with a MFI of 2.0 g/10 min at 230 °C, 2.16 Kg, supplied by Mao Ming Petro-chemistry Co. The POE is Engage 8100 manufactured by Dow Chemical, with an octane-comonomer molar content of 9.8% and a MFI of 1.0 g/10min, at 190 °C, 2.16 Kg. Their densities are 0.9029 and 0.8785 g/cm<sup>3</sup> (measured by MatsuHaku, GH-120M), respectively.

## 2.2 Sample preparation

PP and POE were dried in an oven at 85 °C and 50 °C for 12 h prior to the processing, respectively. Each stratified sample was co-extruded as a sheet about 1.3 mm thick and 25 mm wide by using the multilayered micro-co-extrusion system designed by our lab, the schematic of which is illustrated in Fig. 1. PP melt and POE melt were simultaneously extruded from two different extruders, and combined as 2-layer melt in the co-extrusion block, and then the 2-layer melt flowed through a series of layer multiplying elements (LMEs). In a LME, the melt was sliced into two left and right sections by a divider, and then recombined vertically. An assembly of  $n$  LMEs could produce a multilayered blend with  $2^{(n+1)}$  layers. In this work, 8-, 64- and 128-layer samples were extruded with 2, 4, and 6 LMEs, respectively. The multilayered sheets with different POE volume content were produced by controlling the PP/POE feeding ratio. In the processing, the extruder temperature was 160-180-190-200-200 °C of PP section and 90-180-190-200-200 °C of POE section, respectively. In comparison, conventional PP/POE blends were prepared by mixing equal mass fraction of 8-, 64- and 128-layer multilayered samples with the same PP/POE feeding ratio. The mixing condition was 30 rpm/min for 8 min at 200 °C. The neat PP samples were also prepared under the same shearing force history by using one of extruders in the multilayered co-extrusion

system with 0, 2, 4, and 6 LMEs. The average thickness of the PP or POE layer was calculated by averaging the individual PP or POE layer thickness of the co-extrusion sheets, which was obtained by measuring the POM micrograph of the multilayered samples with the Image-Pro-Plus soft. Table.1 shows the sample code, total sheet thickness, average PP or POE layer thickness, and total POE volume content in the multilayered and conventional blends, which could be calculated from the following formula:

$$V_{POE} = \frac{\rho_B - \rho_{PP}}{\rho_{POE} - \rho_{PP}} \quad (1)$$

where,  $V_{POE}$  is the volume fraction of POE ;  $\rho_B$  is the density of the blends;  $\rho_{PP}$  and  $\rho_{POE}$  represent the densities of neat PP and POE,

**Table1 Sample code, total sheet thickness, average thickness of PP and POE layers, and total POE content of alternating multilayered and conventional blends**

Sample code	Total sheets thickness (μm)	Average PP layers thickness (μm)	Average POE layers thickness (μm)	POE content (Vol%)	
Neat PP	C0, C0-8, C0-32, C0-128	1280	—	—	0
Conventional blends	C1	—	—	—	6.79
	C2	—	—	—	16.57
Alternating multilayered blends	A1-8	1340	311.2	23.1	6.80
	A1-32	1330	77.3	5.5	6.91
	A1-128	1250	18.2	1.3	6.71
	A2-8	1390	289.4	57.3	16.53
	A2-32	1360	70.4	14.8	16.98
	A2-128	1225	16.6	3.4	16.21

respectively. The densities of  $\rho_B$ ,  $\rho_{PP}$  and  $\rho_{POE}$  were measured through a high precision density tester (MatsuHaku, GH-120M). The blends are coded according to the abbreviation for alternating multilayered blends “A”, the number of the layer and the volume content of POE. For example, A2-128 represents the 128 layers multilayered blend with 16.21 Vol% POE. As for the conventional blends and neat PP, the abbreviation is “C”.

### **2.3 Molecular orientation, crystalline characterization**

To eliminate the effects of molecular orientation, crystalline differences on the testing and the remove shearing history, before mechanical test, except some comparison samples, all samples were put into a compress machine with the condition, which is under 10 MPa for 10 min at 200 °C (for imitating the hot-press condition). (More information can be obtained from the Supplementary Information)

### **2.4 Mechanical properties tests**

#### **2.4.1 Notched Izod impact test**

The notched Izod impact strength of the specimens was measured with a XJU-22 Izod machine according to GB/ 1943-2007. In order to understand the impact behaviors clearly, two kinds of layer arrangements  $80 \times 10 \times 4$  mm-thick impact bars were prepared. The alternating multilayered sheets were firstly cut into  $80 \times 15 \times 1.3$  mm-thick sheets and followed were hot-pressed into  $80 \times 15 \times 4$  mm-thick,  $80 \times 15 \times 10$

mm-thick, respectively, the hot-pressed condition is under 10 MPa for 10 min at 200 °C. As shown in Fig. 2, the 80×15×4 mm-thick bars were polished into 80×10×4 mm-thick for the impact paralleled to the layer plane (Fig. 2 (B)); the 80×15×10 mm-thick bars were polished into 80×10×4 mm-thick for the impact vertical to the layer plane (Fig. 2 (A)). Then the obtained samples were added the suffix with the “P” and “V”, which mean that the impact is parallel and vertical to the layer plane, respectively. As for the neat PP and conventional blends, 80×10×4 mm-thick bars were hot-pressed directly for the impact test (Fig. 2 (C)). The depth of the notch is 2 mm. Testing was carried out at ambient temperature (23°C). Each impact test included at least 5 parallel experiments, and the results were averaged.

#### **2.4.2 No-notched impact tensile test**

As shown in Fig. 3, the testing geometry was cut from the centre of the heat treated samples. Impact tensile of the samples was carried out through an instrument XJ-50 (JJ-TEST, China) impact pendulum machine, according to the GB/T13525. The impact velocity was 3.8 m/s. The impact energy was 15 J. Testing was carried out at ambient temperature (23°C). Each impact test included at least 8 parallel experiments, and the results were averaged.

#### **2.4.3 Tensile test**

The standard dog-bone tensile sheets were cut from the centre of

the heat treated samples. Tensile tests were carried out through the extrusion direction at  $10 \text{ mm/min}^{-1}$ . At least five parallel samples were tested in each test.

## 2.5 Polarized optical microscopy (POM) observation

To examine the structure morphologies of multilayered with different layers, a rotary microtome (YD-2508B) microtome was used to cut a  $20 \mu\text{m}$  slice from the multilayered sheets along the transverse direction. The sample slice was placed between two glass slices and then inspected on polarized optical microscopy (POM, Leica, DM2500P)

In order to understand the fracture and toughening mechanism of multilayered and conventional blends, the crack initiation and propagation stage were observed through a part-impact test, which was performed with the XJU-22 impact test machine. The pendulum was raised at an angle of  $30^\circ$  from the vertically fixed specimen, and then released to hit the specimen with appropriately constant impact energy of about 0.3 J. The specimen was not broken into two halves as expected, and the propagating crack or craze stopped in the interior of the specimen. The initiation and propagation patterns of crack or craze were collected by transmission optical microscopy (TOM), with the  $20 \mu\text{m}$  sample slices cut from part-impact specimens along the crack propagation direction but paralleled to the impact direction. The pictures collected by TOM were all recorded with a Pixelink camera (PL-A662).

## 2.6 Scanning electron microscopy (SEM)

The impact fracture behaviors of the samples were also investigated by SEM (JSM-5900LV, Japan). The impact-fracture surfaces were obtained from the notched Izod impact testing. To observe the sub-damage zone (stress whitening zone) underneath the impact-fracture surfaces, the impacted samples were cryogenically polished along the extrusion direction but perpendicular to the layer plane with a tungsten knife at  $-110\text{ }^{\circ}\text{C}$  through the Leica RM2265 microtome (as shown in Fig. 2 (a), (b) and (c)). The impact tensile samples were also polished in same way. Before SEM characterization, all the surfaces were sputter-coated with a gold layer.

## 3. RESULTES AND DISCUSSION

### 3.1 Phase morphology

The most significant difference between the multilayered and conventional blends with the same POE content can be understood reasonably as follows: through the multilayered co-extrusion technology, the alternating multilayered microstructure of the PP layers and the POE layers was successfully fabricated, which can be well observed through the POM images presented in Fig. 4. The macro-anisotropy in the multilayered samples is very obvious and the continuity of each layer is very well. The darker layers in the images belong to the amorphous POE layers, whereas the brighter layers belong to the crystalline PP layers.

Moreover, all of the multilayered samples have a clear laminar morphology, which the PP and POE layers align alternately vertical to the interfaces and continuously parallel to the extrusion direction. It should be noted that the laminar morphology of the A1-128 seems not very clear. It is ascribed that the thickness of POE layers in A1-128 is too low to be distinguished through the POM, while its well continuously laminar morphology can be demonstrated clearly through the SEM of its impact fracture surface (Figures. 7, 8 and 9). As for the conventional blends (C1 and C2), the addition of POE seems to decrease the sizes of the PP spherulites. Given the unique micro-structure of the multilayered samples can greatly influences the PP/POE toughening systems, investigations from macroscopic perspective and microscopic perspective will be conducted in detail later.

### **3.2 Crystalline structure and molecular orientation**

The multilayered PP/POE blends with different layer numbers can be fabricated with different LMEs. More LMEs mean much stronger shearing force that the multilayered blends will suffer from, resulting in distinct differences of crystalline structure and molecular orientation, which will have evident effects on the toughness of the PP/POE system [36, 37]. As the major goal in this work is to investigate whether the alternating multilayered micro-structure can toughen the PP/POE blends, therefore, it is necessary to eliminate the shear and thermal history of the

samples. Just as shown in the Supplementary Information, the thermal treatment condition, which was under 10 MPa for 10 min at 200 °C, indeed removed the shear and thermal history.

### 3.3 Mechanical testing

As indicated in Fig. 5 (a), the notched Izod impact strength of the PP/POE multilayered blends increases with increasing their layer number. Moreover, the Izod values, which are measured vertical to the layer plane direction, are higher than those who are measured parallel to the layer plane direction. It's no obvious variation of Izod values for the neat PP (C0) (about 31.1KJ/m<sup>2</sup>) with increasing its layer number. In detail, the impact strengths of alternating multilayered blends A1-128-V (91.1 KJ/m<sup>2</sup>), A1-32-V (76.9 KJ/m<sup>2</sup>), and A1-8-V (69.6 KJ/m<sup>2</sup>) are 2, 1.7 and 1.5 times as high as that of their corresponding conventional blend C1 (46.5 KJ/m<sup>2</sup>), respectively. While the impact strengths of A1-128-P (69.6 KJ/m<sup>2</sup>), A1-32-P (51.5 KJ/m<sup>2</sup>), A1-8-P (44.1 KJ/m<sup>2</sup>) are only 1.5, 1.1 and 0.95 times as high as that of C1 (46.5 KJ/m<sup>2</sup>), respectively. All these results indicate that no matter parallel or vertical to the layer plane, the multilayered blends with low POE content (6.79 Vol %) and high layer number exhibit higher toughness than their conventional blend. While for the high POE content (16.57 Vol%) multilayered system, although the impact strengths increase slightly with increasing their layer number, except A2-128-V, the Izod values of the others are slightly lower than that

of their corresponding conventional blend. As for the no-notched impact tensile strength, the impact tensile strengths of multilayered blends enhance obviously by increasing their layer number (Fig. 5 (b)). For the low POE content system, the impact tensile strengths of alternating multilayered blends A1-128 (781.3 KJ/m<sup>2</sup>), A1-32 (442.0 KJ/m<sup>2</sup>), and A1-8 (381.8 KJ/m<sup>2</sup>) are about 1.8, 1 and 0.86 times as high as that of their conventional blend C1 (443.8 KJ/m<sup>2</sup>), respectively. For the high POE content system, the impact tensile strengths of alternating multilayered blends A2-128 (855.6 KJ/m<sup>2</sup>), A2-32 (666.2 KJ/m<sup>2</sup>), and A2-8 (411.7 KJ/m<sup>2</sup>) are about only 1.2, 0.94 and 0.58 times as high as that of their conventional blend C2 (712.0 KJ/m<sup>2</sup>), respectively. The neat PP with different layers present a stable value about 520 KJ/m<sup>2</sup>. Interestingly, compared with C1, A1-8, A1-32 and A2-8, neat PP with different layers exhibit a high impact tensile value. As the multilayered blends present high toughness than their corresponding conventional blends, and the Izod values of the multilayered blends with high POE content are lower than those with low POE content. Therefore, the corresponding toughening mechanisms should be discussed in detail.

On the other hand, the differences of the tensile yield strength of neat PP and the multilayered blends with different layers are little (Fig. 5 (c)). The tensile yield strengths of the multilayered blends, in particular the high POE content system, are higher than those of their corresponding

conventional blends, which is consistent with our previous work [32]. According to equivalent box model, the yield strength of dispersed, co-continuous structure would be lower than those with multilayered structure [38, 39].

### 3.4 Fracture and toughening mechanisms

The photographs of Izod samples taken after the notched impact test often give some macroscopic information to understand the toughening mechanisms. As shown in the Fig. 6 (a), the neat PP (C0) and conventional blends (C1, C2) exhibit a hinged breakage and a semi-circle stress whitening zone. As for the multilayered blends, when measured parallel to the layer plane, the semi-circle stress whitening zone is also found, while only the A2-8-P and all low POE content system (A1) exhibit obviously hinged breakage. When the samples are measured vertical to the layer plane, except a large rhombus-shaped stress whitening zone, no obvious breakage can be found. In order to analyze the differences of the stress whitening zone between conventional and multilayered blends, some of the photographs shown in the Fig. 6 (b) are treated by the Image-Pro-Plus soft with the Invert Contrast Model, where the black zone correspond to the stress whitening zone in the Fig. 6 (a). Stress whitening, the tendency of polymer materials to display a white appearance under imposed stress, is ascribed to the scattering entities or localized stress concentration sites scatter light. For PP and

PP/elastomer blends, stress whitening is caused by the crazes and micro-voids during the deformation process [40, 41].

The total energy of fracture can be partitioned into two components; (i) one is consumed to create new fracture surface, and (ii) the other is dissipated in the stress whitening zone (bulk damage) for the deformation of matrix or dispersed phase. Therefore, most of the fracture energy must be consumed through the bulk damage for the fracture without obvious breakage. Consequently, only the impact fracture surface morphologies of the samples with obvious breakage are inspected by SEM. Figures 7, 8 and 9 show the representative impact fracture surface morphologies of C0, C1, A1-8-P and A1-128-P. As shown in the Figures 7 and 8, the micrographs clearly illustrate three distinct types of fracture morphologies: (a) a relatively smooth zone “A” in the vicinity of the origin or primary crack initiation sites; (b) the coarse zone “B” with many strip-like protrusions and pleats arranging vertical to the impact direction, which represent the plastic deformation zone, and (c) unbroken part zone “C” shown by the rectangular-shaped dashed lines. Most interestingly, the fracture morphologies of the multilayered blends, particularly for the A1-128-P, are characterized by amounts of delaminations of the PP/POE interfaces. It should be noted that the relative smooth region in the left of the unbroken part zone “C” of the A1-128-P was cut through a blade. Generally, good toughness materials can't break completely during the

impact test. Even the C0, there is still some small unbroken zone. What's more, though the POE content is the same, the area of unbroken zone increase by the sequence of A1-8-P, C0, C1 and A1-128-P, which is roughly consistent with their Izod values. In addition, as shown in the high magnification micrograph Fig. 8, there is almost no difference between the C0 and A1-8-P (taken only from PP layer), in the either A zone, surface characters without any obvious plastic deformation and micro-voids, while in the either B zone, the local deformation of the matrix characters with large amounts of protrusions and pleats arranging perpendicular to the impact direction. In comparison with the C0 and A1-8-P, the visualized surface morphologies of the conventional blend C1 are little different. Firstly, the A zone becomes much coarser, and small scale local matrix deformation is found; secondly, one can notice that more visible protrusions and pleats are formed in B zone, which mean much greater local deformation of the matrix, while the voids still not be observed. Besides, the fracture surface of the PP layers in A1-128-P reveals totally different morphologies. The surface, particularly in A zone, is very smooth, and unexpectedly, there is no obvious local deformation in B Zone. More interestingly, although the interfaces exist between PP and POE phase for all blends, delaminations of interfaces are only observed in multilayered blends. It's been proven that the delaminations of interfaces can dramatically enhance the toughness of materials [5, 42,

43]. Consequently, it's highly desirable to inspect the delaminations of the interfaces. As shown in Fig. 9, for the A1-8-P, interfaces delaminations are found in both the A and B zone, while in the A zone, there is nearly no deformation for the POE layers, while in the B zone, the POE layers are deformed into asperities and crumple slightly. In contrast, for the A1-128-P, besides the delaminations between PP and POE layers, the POE layers are torn into fibrils in B zone and into pellets in A zone. The fibrils or pellets are named as "ligaments" and these ligaments bridge across the adjacent PP layers. As mentioned in introduction section, one of the important explanations for the superior toughness of nacre is the energy-dissipating of the 5 Vol% fraction of organic phase (just like the POE phase in PP/POE multilayered blends) through the formation of organic ligaments between platelets [44]. Besides, the ligaments are also found in PLA/PBSA system with a compatibilizer, which finally toughen the PLA/PBS system dramatically [43]. Therefore, the observation of amounts of ligaments in A1-128-P can partially account for its higher toughness. Additionally, the crumple deformation of PP layers in A1-128-P can also consume energy, which may be another contributor for its high toughness.

In order to get more in-depth evidence for understanding the toughening mechanisms, the cross sections beneath the impact fracture surface of the samples are also observed with SEM. As shown in Fig. 10,

the locations, where the micrographs were taken, are the zone underneath the impact fracture surface, 50  $\mu\text{m}$ , 500  $\mu\text{m}$  and 5000  $\mu\text{m}$  away and labeled 1, 2 and 3, respectively (as shown by Fig. 2 (a), (b) and (c)). For the C0, slight shear yielding and few voids are visualized at least 50  $\mu\text{m}$  beneath the fracture surface (C0-1), at the distant 500  $\mu\text{m}$  away, the shear yielding is unobvious while the voids still can be found (C0-2). Moving farther distance leads to the region absolutely unaffected by the fracture surface (C0-3). For the conventional blend C1, moderate intensive shear yielding and voids are observed at least 500 $\mu\text{m}$  (C1-1, C1-2). Both the shear yielding and voids are not apparently in C1-3. As for the high POE content C2, both the intensive shear yielding and extensive elongated voids with bigger sizes are visualized in C2-1. Compared with C2-1, slightly intensive shear yielding and less elongated voids are found in C2-2. Moving farther from the fracture surface also leads to the region affected slightly (C2-3). It's worthy of noting that the small and regular dark spheres in C2-3 are POE particles instead of voids. Generally, under impact stress, the POE particles act as stress concentrator and cavitation sites. After cavitation, the triaxial stress disappears and the matrix behaves as if it were under plane-stress conditions, where more shear yielding readily occurs. Additionally, the voids created by the POE particles further act as the stress concentrator [45]. Therefore, the addition of POE toughens PP by accelerating the

formation of voids and shear yielding, which can be shown well by the Fig. 10 (C0-1~C1-3). In particular, when the POE content is higher than a critical value, the distance between two neighboring POE particles is smaller than the critical matrix ligament thickness. In such case, the overlap of the adjacent stress fields will firstly initiate the local shear yielding in PP matrix, and subsequently result in the deformation of PP matrix, just shown as the Fig. 14 (C2-1, C2-2). The cooperative motion of PP matrix and POE phase consumes large amounts of energy [46, 47], which finally toughen the PP dramatically.

As for the multilayered blends A1 and A2, extraordinary and versatile bulk morphologies are found. In the case that the impact vertical to the layer plane, in the zone 50  $\mu\text{m}$  away beneath the fracture surface, relative smooth surface with only few scattered voids occurs (A1-128-V-1), which is caused by the adiabatic heating process generated during the fracture [5, 48], While in the area further away from fracture surface (500  $\mu\text{m}$  away for A1-128-V-2), the shear yielding becomes obvious, moreover, both the sizes and density of the voids increase dramatically. For the furthest area 5000  $\mu\text{m}$  away (A1-128-V-3), the surface with moderate shear shielding and voids is still visible. In comparison, overall deformation of the PP layers accompanied with the interfaces delaminations can be observed well in A2-128-V-1. Sea-island-like surface caused by the local deformation of the PP layers and strip-shaped

smooth surface are observed in A2-128-V-2. As much thicker of the strip-shaped smooth surface than that in A2-128-V-1, this strip-shaped smooth surface may not only include the POE layers but also the partial PP layers where near to the POE layers. Neither the shear yielding nor the voids are obvious in A2-128-V-3. As the deformation is an adiabatic process during the impact test, considerable stress can be released, which finally results in a relaxation zone with less voids and deformation in the micrographs (Fig. 11). Moreover, the occurrence of the relaxation zone is accompanied with an increase in fracture energy, which may result from its crack blunting effects [48, 49]. Interestingly, the relaxation zone is only present in A1-128-V and A1-128-P, which partially accounts for the high impact strength of the A1-128-V. On the other hand, the formation of voids can toughen materials obviously [50~52]. Additionally, the formation of the voids will consume more energy in homogeneous materials rather than heterogeneous materials as the homogeneous materials usually have higher surface energy. As plenty voids are observed in the homogeneous PP layers and spread over at least 5000  $\mu\text{m}$  away under fracture surface (except for the relaxation zone), which is important contributor for the superior toughness of A1-128-V. Moreover, the large shear yielding zone may be another explanation for its high toughness. As for the A2-128-V, although the overall deformation and delaminations are observed near the fracture surface, the severity of the

deformation decreases sharply with the distance. Additionally, the voids are un conspicuous. In other words, it can be deduced that the lower toughness of A2-128-V than that of A1-128-V results from its smaller subcritical damage region, the absent of relaxation zone and the inability to form plenty of voids.

Versatile bulk morphologies are also found on the condition where the impact direction is parallel to the layer plane. One can observe a peculiar stalactite lava-like morphology with intensive voids in A1-128-P-1. Interestingly, this morphology seems to be in partial relaxation or melting state, which is caused by the adiabatic process during the impact tests (Fig. 11). Obvious shear yielding and voids are observed in A1-128-P-2. As for the furthest region A1-128-P-3, the morphology seems unaffected by the fracture surface. On the other hand, for the A2-128-P, strong shear flow of the PP and POE accompanied with large elongated voids can be readily revealed in A2-128-P-1. Compared with the A2-128-P-1, slightly shear flow is only found in PP layers and the elongation extent of voids decrease while their sizes become bigger in A2-128-P-2. As for the A2-128-P-3, the morphology seems also unaffected by the fracture surface. Just as the above description, the higher unbroken part (As shown by the Fig. 6) and the absent of the relaxation zone in A2-128-P result in its lower Izod value than that of the A1-128-P.

In order to further ascertain the specially impact behaviors of the multilayered blends, POM micrographs from the subcritical damage zone of the part-impact samples are shown in Figure 12. For comparison, POM micrographs of the conventional blend and neat PP are also taken. For the multilayered blends impacted vertical to the layer plane (A1-128-V), a mass of craze deflects along the PP/POE interfaces and only a handful of craze can propagate through the soft POE layers. As for the A1-8-V, only a certain amounts of multiple craze is restricted in only one of the PP layers with a standard rectangular-shaped zone. Interestingly, these craze seems to be initiated from the POE layer, which is located at the crack tip and arrested by the next adjacent POE layer. On the other hand, for the multilayered blends impacted parallel to the layer plane (A1-8-P and A1-128-P), massive craze is initiated around the crack tip and then propagates along to the impact direction. Finally, a fan-shaped craze zone is formed. Unlike the A1-128-V, craze deflection is observed not only near the crack tip but also at the root of crack in A1-128-P. However, one may question the rationality of the occurrence of craze deflection in the POM micrograph of A1-128-P because the slice for POM is taken parallel to the layer plane in A1-128-P. In fact, it's difficult in taking the slice only from one of the layers as the thin layer in A1-128-P. Because the thicker PP layers in the A1-8-P, the effects of the POE layers can be negligible for those craze initiation sites are far enough, which results in

the similar craze patterns of the C0 and the A1-8-P. Compared with the C0, large multiple craze (much large dark zone) is observed for the conventional blend (C1) indicating the incorporation of the POE can toughen the materials by accelerating the generation of massive craze. As craze prone to propagating along the weakness of materials [53], most of the fracture energy must be dissipated though the craze deflecting along to the weak PP/POE interfaces in A1-128-V. Besides, the existence of the soft POE layers can blunt the craze though their deformation. In simple words, the effects of the soft POE layers on the crazing behaviors of the multilayered blends are to provide a deflection interfaces and blunt the craze, so that craze has more difficulty in propagating through the layers. The A1-8-V still presents high toughness despite its low layer number since the craze in A1-8-V can be perfectly arrested by the adjacent thick and soft POE layer, in addition, more craze initiation sites are formed along the interfaces, which can prevent the transformation of damage from craze to crack, and finally avoid the catastrophic fracture of the multilayered materials. When the impact is parallel to the layer plane, the craze pattern of the A1-8-P is similar to that of the C0 and this can account for its poor impact strength well. Compared with the A1-8-P, craze deflection is also found in A1-128-P. Most importantly, plenty of interfaces delaminations are found at its fracture surface (Fig. 7). All these factors act over toughening the multilayer materials and finally

endow the A1-128-P with high toughness than those of the A1-8-P and C1.

We have to admit some of the samples can't break completely during Izod impact test. So the Izod values of those not broke completely samples can't fully reflect their toughness. In order to reflect the toughness of all samples comprehensively, the impact tensile test was also carried out. Just as shown in Fig. 13, the fracture surface morphologies and the bulk morphologies underneath the fracture surface were also inspected by SEM. The fracture surface of the A1-128 is smooth (Fig. 13 (A)). More information can be revealed through the close-up of the rectangular dashed zones in A1-128 (Fig. 13 a1 and a2). The surface of the a1 is rather smooth while slight delaminations and ductile tearing align parallel to the layer plane in the surface of a2. For the A1-8, smooth fracture surface is also observed (Fig. 13 (B)). Although obvious delaminations are observed in right edge of the fracture surface, most of the interfaces still keep perfect just as shown in the close-up b2. As for its PP layers, slight deformation arranges horizontally and ductile tearing arranges vertically downward (b1). Similar but more severe deformation and ductile tearing are observed in the c1. In addition, smooth surface with few voids is illustrated in the c2. Compared with the blends, the most distinct difference of the C0 (Fig. 13 (D)) is the "necking" during the fracture process, which can mainly account for its

high impact tensile value. As for its fracture surface, coarser surface with little voids is found in d1 while smooth surface without the voids is formed in d2. Although the samples exhibit complicated fracture surfaces, it's clear that the information from the fracture surface can't fully account for their distinct impact tensile performances. Herein, it's necessary to reveal the bulk morphologies underneath the fracture surfaces (Fig. 13 (A1~D3)). For the A1-128, obvious delaminations and warping PP layers with few voids are observed at least 100  $\mu\text{m}$  beneath the fracture surface (Fig. 13 (A1)). Severe local deformation and voids are observed at 700  $\mu\text{m}$  beneath the fracture surface (Fig. 13 (A2)). Moving further distance, only plenty of voids with bigger sizes are found (Fig. 13 (A3)). In comparison, in A1-8, delaminations are absent and the voids are obvious at least 100  $\mu\text{m}$  beneath the fracture surface (Fig. 13 (B1)). Moreover, away from the fracture surface, the severity of the plastic deformation decreases, massive plastic deformation can be observed at least 100  $\mu\text{m}$  beneath the surface, whereas the local plastic deformation can be observed at the distance of 700  $\mu\text{m}$  and 2000  $\mu\text{m}$  away underneath the fracture surface (Fig. 13 (B1~B3)). On the other hand, for the C1, slight local deformation and voids can be seen at least 700  $\mu\text{m}$  underneath the surface (Fig. 13 (C1~C2)), moving farther distance resulting an absolutely unaffected bulk morphology by the fracture surface (Fig. 13 (C3)). As for the C0, at the distance 700 $\mu\text{m}$  away from the fracture

surface, an apparent boundary lay between the deformation zone and the smooth zone (Fig. 13 (D2)). The morphology before the boundary belongs to the necking zone with obvious deformation (Fig. 13 (D1)). Beyond the necking zone, the morphology seems not to be affected during the impact test (Fig. 13 (D3)). By combining the analysis of fracture surface morphologies and the bulk morphologies, it can be deduced that the higher impact tensile strength of the A1-128 results from its versatile bulk morphologies, which can be characterized with delaminations, sever local deformation, plenty of voids and the formation of ductile tearing in fracture surface. Compared with the A1-8, the C1 is characterized with severer deformation and apparently ductile tearing at the fracture surface but a small bulk damage zone beneath the fracture surface. Therefore, the A1-8 and C1 present proximate impact tensile value. As for the C0, the “necking” phenomenon of C0 leads to its higher impact tensile value. As the impact tensile strength of the high POE content system, the similar morphologies characters are also observed (not shown in here), which can also interpret the difference of their impact tensile performance.

### **3.5 Structure and property relations**

Base on the above discussion, we herein attempt to summarize the influences of the soft and stiff alternating multilayered structure on the mechanical properties of the PP/POE blends, in particular the Izod impact

strength. Schematic illustration is proposed for the craze patterns of the typical multilayered blends (Fig. 14 (a ~ c)), and conventional blend C1 (Fig. 14 (d)). For the A1-128-V, most of fracture energy is consumed through craze deflecting along to PP/POE interfaces, besides, the existence of the soft POE layers can blunt the craze through its deformation as the craze propagation direction vertical to the layer plane (Fig. 14 (a)), which facilitate the enhancement of impact toughness. In the case of less layers multilayered blends A1-8-V, although the craze deflection is invisible, more craze initiation sites are found along the PP/POE interfaces and the initiated craze is perfectly arrested by the next adjacent POE layer (Fig. 14 (b)), which also enabled the enhancement of its impact toughness. As for the A1-128-P and C1, it's no obvious difference in the amounts of the craze except the shape of craze zone. Therefore, the corresponding toughening mechanism will be revealed by the combination analysis of the fracture surface morphologies and bulk morphologies as shown in the schematic Fig. 15. The neat PP (C0) and the conventional blend C1 exhibit the same sort of morphologies, indicating the same fracture mechanism of them. While in detail, much remarkable protrusions, pleats and the unbroken part are found in the fracture surface of the C1 (Fig. 15 (A), (B)), at same times, much large sub-damage zone with extensive shear deformation and voids are also formed in C1 (Fig. 15 (a), (b)). Such morphologies characteristics result

in the ultimate toughness enhancement of C1 than that of C0. Compared with the C1, the most distinct fracture surface morphologies of A1-128-P are the PP/POE interfaces delaminations (Fig. 15 (C)). Besides, near the fracture surface, a relaxation zone with smooth bulk morphology is formed (Fig. 15 (c)). Just as the discussion in section 3.4, the occurrence of the relaxation zone and delaminations lead to the high toughness of the A1-128-P. Compared with the A1-128-P, although the A2-128-P presents severer shear deformation, much bigger sizes voids and nearly same large sub-damage zone (Fig. 15 (d)), the relaxation zone is absent. In addition, due to the little breakage of the A2-128-P (Fig. 6) during impact testing, the new fracture surface created by the fracture process is little and the interfaces delaminations, if exist, should be also little. All these result in its low Izod value than that of A1-128-P despite its high POE content. On the other hand, the relative smooth surface morphology caused by the relaxation zone near to the fracture surface, the large sub-damage zone (at least 5000  $\mu\text{m}$  away from the impact fracture surface) and the plenty of big sizes voids in a moderate distance are developed during the impact testing, which finally enabled the superior impact strength of A1-128-V (Fig. 15 (e)). As for A2-128-V, its sub-damage is small and the relaxation zone is absent what's more, the delaminations and obvious plastic deformation is concentrated close to the fracture surface (Fig. 15 (f)), which facilitate the A2-128-V with a poorer impact strength than that of

A1-128-V despite its high POE content.

Although the soft and stiff alternating multilayered structure has been proven to be efficient to toughen the PP blends in this work, the toughness of the multilayered blends is enhanced 2 times as high as that of their corresponding conventional blends with proper POE content and impact direction, which is far not as outstanding as nacre. Therefore, many challenges still need to be overcome. Firstly, we have to admit that the synergic factors that act over multiple scales to toughen nacre are only partially observed in PP/POE multilayered blends. Additionally, it's really a great challenge to copy the multiscale fine features of nacre, such as platelet waviness, mineral bridges and nano-asperities through the micro-co-extrusion. Moreover, the toughness of polymers change widely and for those possess quite toughness polymers the potential improvement of the toughness cannot be as outstanding as the inorganic materials such calcium carbonate in nacre or ceramics in layer ceramics. Therefore, we wonder if a relative "brittle" material is chosen, or the toughness measured in a lower temperature, whether more outstanding improvement of the toughness can be gained with the multilayered microstructure. This work is now being undertaken in our group.

#### **4. CONCLUSION**

In this work, two different POE contents (6.79 and 16.57 Vol%) multilayered blends were successfully fabricated and the shear history of

the blends was successfully removed through the heat treatment. Compared with the conventional blending samples, no matter that the impact is vertical or parallel to the layer plane, the alternating multilayered blends with low POE content and high layer number present high Izod impact values. At the same times, the impact tensile strength of the multilayered blends with high layer number also present high values. It is ascribed to the unique fracture mechanisms during the fracture process. In detail, the craze deflects along the PP/POE interfaces, large sub-damage zone and the occurrence of the relaxation zone can main account for their high toughness. As the high POE content multilayered blends, the inefficiency to form voids as well as the absent of the relaxation zone and the small sub-damage zone lead to their low Izod value. As the abnormal phenomena that the multilayered blends with low POE content exhibit high toughness, this work provides us not only a deep insight for understanding the toughening mechanism but also a new route to toughen PP or other polymer materials without sacrificing their strength obviously.

#### **ACKNOWLEDGEMENTS**

Financial supports of the National Natural Science Foundation of China (51273132, 51227802 and 51121001) and Program for New Century Excellent Talents in University (NCET-13-0392) are gratefully acknowledged.

**REFERENCES**

- (1) W. V. Vander, R. Nijhof and R. J. Gaymans, *Polymer* 1999, 40, 6031-6044.
- (2) C. M. Chan, J. S. Wu, J. X. Li and Y. K. Cheung, *Polymer* 2002, 43, 2981-2992.
- (3) D. Shah, P. Maiti, E. Gunn, D. F. Schmidt and D. D. Jiang, *Adv. Mater.* 2004, 16, 1173-1177.
- (4) W. C. J. Zuiderduin, C. Westzaan, J. Huetink and R. J. Gaymans, *Polymer* 2003, 44, 261-275.
- (5) Y. Lin, H. Chen, C. M. Chan and J. Wu, *Macromolecules* 2008, 41, 9204-9213.
- (6) L. P. Li, B. Yin and M. B. Yang, *Polymer* 2012, 53, 3043-3051.
- (7) O. Masami and S. Yoshihiro, *Polymer*, 1993, 23, 4868-4873.
- (8) X. L. Gao, C. Qu, Q. Zhang and Q. Fu, *Macromol. Mater. Eng.* 2004, 1, 41-48.
- (9) L. Hyuksoo, D. F. Paula and R. R. William, *Polymer* 2005, 46, 11673-11689
- (10) D. A. Stone, and L. T. J. Korley, *Macromolecules* 2010, 43, 9217-9226.
- (11) M. A. Meyers, P. Y. Chen, A. Y. M. Lin and Y. Seki, *Prog. Mater. Sci.* 2008, 53, 1-206.

- (12) T. H. Lin, W. H. Huang, I. K. Jun, and P. Jiang, *J. Colloid Interface Sci.* 2010, 344, 272–278.
- (13) R. Libanori, F. H. L. Munch, D. M. Montenegro and A. R. Studart, *Compos. Sci. Technol.* 2012, 72, 435-445.
- (14) L. J. Bonderer, A. R. Studart and L. J. Gauckler, *Science* 2008, 319, 1069–1073.
- (15) L. J. Bonderer, K. Feldman and L. J. Gauckler, *Compos. Sci. Technol.* 2010, 70, 1966–1972.
- (16) L. J. Bonderer, K. Feldman, and L. J. Gauckler, *Composites Compos. Sci. Technol.* 2010, 70, 1958–1965.
- (17) I. Corni, T. J. Harvey, J. A. Wharton, K. R. Stokes, F.C. Walsh and R. J. K. Wood, *Bioinspiration Biomimetics* 2012, 7, 031001.
- (18) C.D Mueller, S Nazarenko, T. Ebeling, T. L. Schuman, A. Hiltner and E. Baer, *Polym. Eng. Sci.* 1997, 37, 355-362.
- (19) M. Gupta, Y. J. Lin, D. Taneisha, A. S David and E. Baer, *Macromolecules* 2010, 43, 4230-4239.
- (20) R. Tangirala, E. Baer, A. Hiltner and C Weder, *Adv. Funct. Mater.* 2004, 14, 595-604.
- (21) S. X. Xi, M. Wang, J. Li and S.Y. Guo, *Polymer* 2008, 49, 4861-4870.
- (22) E. Baer, A. Hiltner and H. Keith, *Science* 1987, 235, 1015-1022
- (23) E. Shin, A. Hiltner and E. Baer, *J. Appl. Polym. Sci.* 1993, 47, 269-288.

- (24) D. Haderski, K. Sung, A. Hiltner and E. Baer, *J. Appl. Polym. Sci.* 1994, 52,121-133.
- (25) K. Sung, D. haderski, A. Hiltner and E. Baer, *J. Appl. Polym. Sci.* 1994, 52,135-146.
- (26) K. Sung, D. haderski, A. Hiltner and E. Baer, *J. Appl. Polym. Sci.* 1994, 52, 147-162.
- (27) J. Kerns, A. Hsieh, A. Hiltner and E. Baer, *J. Appl. Polym. Sci.* 2000, 77, 1545-1557.
- (28) T. M. Burt, J. Keum, A. Hiltner and E. Baer, *ACS Appl. Mater. Inter* 2011, 3, 4804-4811.
- (29) T. M. Burt, A. M. Jordan and T. J. K. Korley, *ACS Appl. Mater. Inter* 2012, 4, 5155-5161.
- (30) J. Kerns, A. Hsieh, A. Hiltner and E. Baer, *Macromolecular Symposia* 1999, 147, 15-25.
- (31) J. B. Shen, M. Wang, J. Li and S. Y. Guo, *Eur. Polym. J.* 2009, 45, 3269-3281.
- (32) J. F. Wang, C. L. Wang, X. L. Zhang and H. Wu, *RSC Adv.* 2014, 4, 20297-20307.
- (33) J. D. Currey, *Proc. R. Soc. London. Ser. B* 1977, 196, 443-463.
- (34) A. P. Jackson, J. F. V. Vincent and R. M. Turner, *Proc. R. Soc. London. Ser. B* 1988, 234, 415-440.

- (35) R. Z. Wang, H. B. Wen, F. Z. Cui and H. B. Zhang, *J. Mater. Sci.*, 1995, 30, 2299-2304.
- (36) C. Z. Gen, J. J. Su, S. J. Han, K. Wang and Q. Fu, *Polymer* 2013, 54, 3392-3401.
- (37) J. B. Bao, T. Liu, L. Zhao and G. H. Hu, *Ind. Eng. Chem. Res.* 2011, 50, 9632-9641.
- (38) L. E. Nielsen and E. Lawrence, London: Reinhold Publishing Corporation; 1962.
- (39) J. Kolarik, *Polymer* 1996, 37, 887-891.
- (40) Y. Liu, C. H. L. Kennard, R. W. Truss and N. J. Calos, *Polymer* 1997, 38, 2797-2805.
- (41) A. Dasari and R. D. K. Misra, *Acta Materialia* 2004, 52, 1683-1697.
- (42) H. Tan, Y. Huang, C. Liu, G. Ravichandran, H. M. Inglis and P. H. Geubelle, *Int. J. Solids. Struct.* 2007, 44, 1809-22.
- (43) O. Vincent, S. R. Suprakas and S. Rotimi, *ACS Appl. Mater. Inter.* 2012, 4, 6690-6701.
- (44) G. Mayer and M. Sarikaya. *Exp. Mech.* 2002, 42, 395-403.
- (45) W. G. Perking, *Polym. Eng. Sci.* 1999, 39, 2445-2460.
- (46) J. Z. Liang and R. K. Y. Li, *J. Appl. Polym. Sci.* 2000, 77, 409-417.
- (47) G. Yang, L. Han, H. Ding, H. Wu, T. Huang and X. Li, *Mater. Sci. Eng. A* 2011, 528(3), 1382-1390.

- (48) A. Wal, and R. J. Gaymans, *Polymer* 1999, 40, 6067-6075.
- (49) K. Dijkstra and R. J. Gaymans, *J. Mater. Sci.* 1994, 29, 3231-3238.
- (50) A. Pawlak and A. Galeski, *Macromolecules* 2008, 41, 2839-2851
- (51) H. W. Bai, H. Xiu , J. Gao , H. Deng , Q. Zhang , M. B. Yang and Q. Fu, *ACS Appl. Mater. Interfaces* 2012, 4, 897-905.
- (52) A. Dasari, Q. X. Zhang, Z. Z. Yu and Y. W. Mai, *Macromolecules* 2010, 43, 5734-5739.
- (53) J. Sun and B. Bhushan, *RSC Advances*. 2012, 2, 7617-7632.

### **Illustration for the numbered graphics of the revised manuscript**

Fig. 1 Sketch of multilayered co-extrusion technology: A, B-single screw extruder; C-connector; D-layer multiplying element (LME); E-die.

Fig. 2 Schematic representation of impact test through different directions of alternating multilayered and conventional blends and the position for the SEM. (A) alternating multilayered blends impact vertical to the layer plane; (B) alternating multilayered blends impact paralleled to the layer plane; and (C) conventional blends and neat PP. (1, impact direction; 2, guide chute; 3, fixed clamp). (a), (b) and (c) illustration for SEM position.

Fig. 3 Schematic representation of impact tensile test

Fig. 4 Polarized optical micrographs of the conventional and multilayered blends morphologies.

Fig. 5 Mechanical properties of the alternating multilayered, conventional blends and neat PP. (a): notched Izod impact strength though different directions; (b) no-notched impact tensile strength; (c): tensile yield strength.

Fig. 6 Photographs of Izod samples taken after the notched impact test (a: normal photographs; b: typical photographs treated by the Image-Pro-Plus soft with the Invert Contrast Model)

Fig. 7 SEM images of the impact fracture surface of neat PP (C0), conventional blend (C1) and the multilayered blends (A1-8-P and A2-128-P) at low magnification. A, B indicates the crack initiation zone, and crack propagation zone, respectively. The zone C marked by rectangular-shaped dashed line represents the unbroken part of the samples during the impact fracture process.

Fig. 8 SEM images of the impact fracture surface of neat PP (C0), conventional blend (C1) and the multilayered blends (A1-8-P and A2-128-P) at high magnification. The images were obtained from the different zones shown in Figure. 7. For the A1-8-P, the images were taken from the PP layers. The scale bars present 20  $\mu\text{m}$ .

Fig. 9 SEM images of the interfaces delaminations from the impact fracture surface of the multilayered blends (A1-8-P and A2-128-P) at high magnification. The images were obtained from the different zones shown in Figure. 7. The scale bars present 50  $\mu\text{m}$ .

Fig. 10 SEM micrographs of the cross sections underneath the impact fracture surface of the neat PP (C0), conventional blends (C1 and C2) and multilayered blends (A1-128-V, A1-128-P, and A2-128-V, A2-128-P). The scale bars present 20  $\mu\text{m}$ . The location, from where the micrographs were taken, are the zone under the impact fractured surface, 50  $\mu\text{m}$ , 500  $\mu\text{m}$  and 5000  $\mu\text{m}$  away and labeled 1, 2 and 3, respectively.

Fig. 10 Continued...

Fig. 11 SEM micrographs of the cross sections underneath the impact fracture surfaces of the A1-128-V and the A1-128-P, the fracture surface

locates at the left. The dashed zone presents the relaxation zone, which formed during the impact process.

Fig. 12 Craze initiation patterns of the samples after the Izod notched part-impact test. (C0: neat PP; C1: conventional blend; A1-8-P and A1-128-P: multilayered blends impacted paralleled to the layer plane; A1-8-V and A1-128-V: multilayered blends impacted vertical to the layer plane).

Fig. 13 SEM images of the no-notched impact tensile fracture surface morphologies and the bulk morphologies beneath the fracture surface of the multilayered blends (A1-8 and A1-128), conventional blend (C1) and the neat PP (C0) at different magnification. For the low and high magnification, the scale bars present 2 mm and 50  $\mu\text{m}$ , respectively. The subscript 1, 2 and 3 of the A1~D3 presents 100  $\mu\text{m}$ , 700  $\mu\text{m}$  and 2000  $\mu\text{m}$  away from the fracture surface, respectively.

Fig. 14 Schematic for the craze patterns of the typical multilayered and conventional blends during the part-impact test. (a): A1-128-V; (b): A1-8-V; (c): A1-128-P; (d):C1.

Fig. 15 Schematic illustrations for the fracture surface morphologies and

the bulk morphologies beneath the fracture surface. A~B present the fracture surface of C0, C1 and A1-128-P, respectively. a~f present the bulk morphologies beneath the fracture surface 50 $\mu\text{m}$ , 500 $\mu\text{m}$  and 5000 $\mu\text{m}$  away. ((A), (a): C0; (B), (b): C1; (C), (c): A1-128-P; (d): A2-128-P; (e): A1-128-V and (f): A2-128-V).

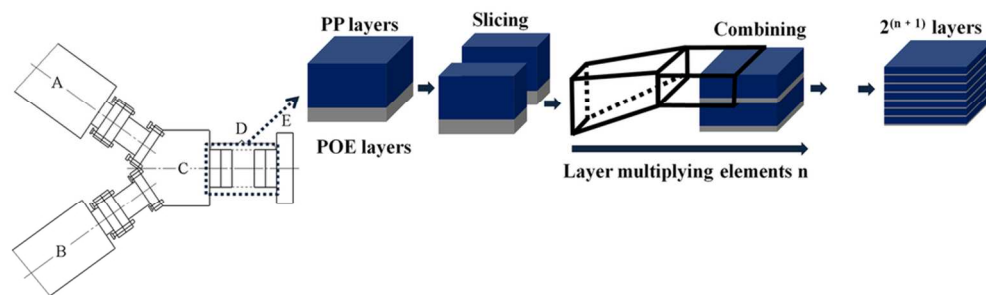


Fig. 1 Sketch of multilayered co-extrusion technology: A, B-single screw extruder; C-connector; D-layer multiplying element (LME); E-die.  
45x13mm (600 x 600 DPI)

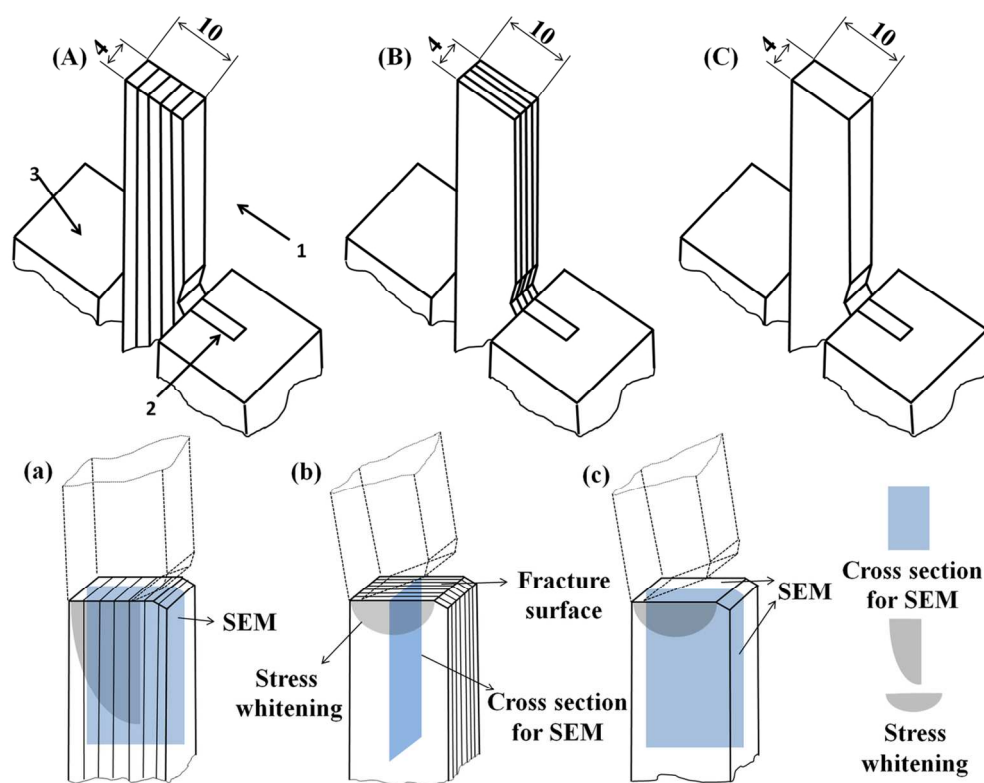


Fig. 2 Schematic representation of impact test through different directions of alternating multilayered and conventional blends and the position for the SEM. (A) alternating multilayered blends impact vertical to the layer plane; (B) alternating multilayered blends impact paralleled to the layer plane; and (C) conventional blends and neat PP. (1, impact direction; 2, guide chute; 3, fixed clamp). (a), (b) and (c) illustration for SEM position.

59x47mm (600 x 600 DPI)

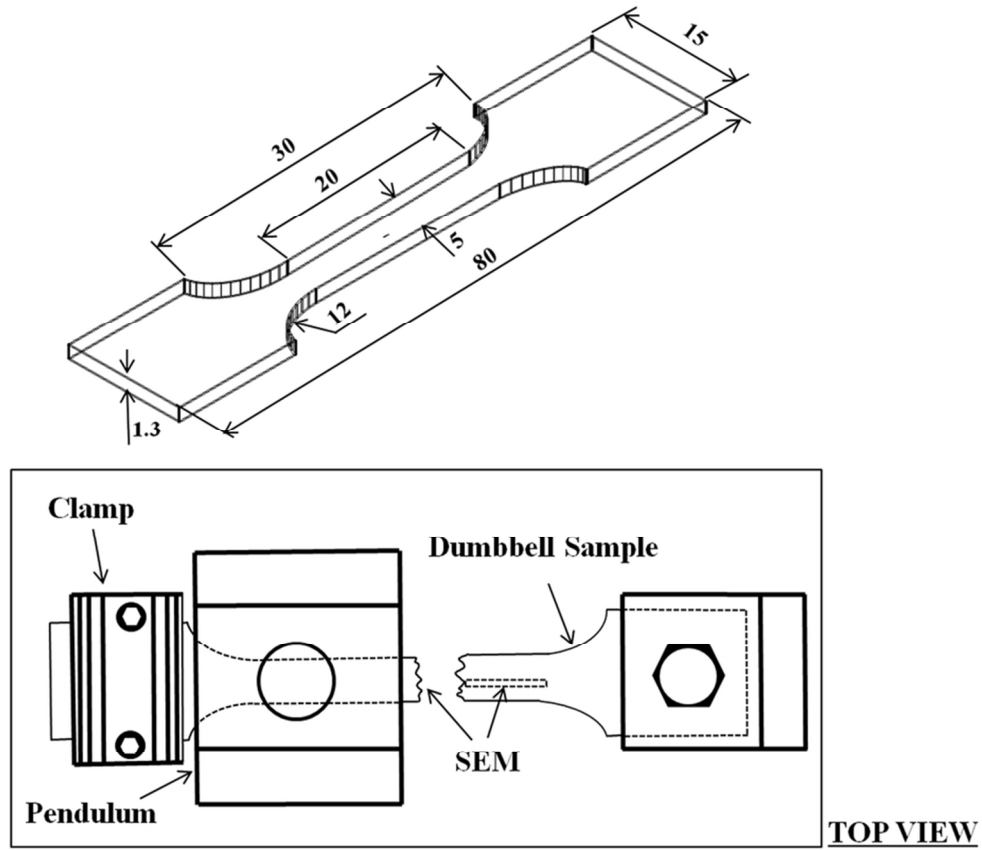


Fig. 3 Schematic representation of impact tensile test  
40x34mm (600 x 600 DPI)

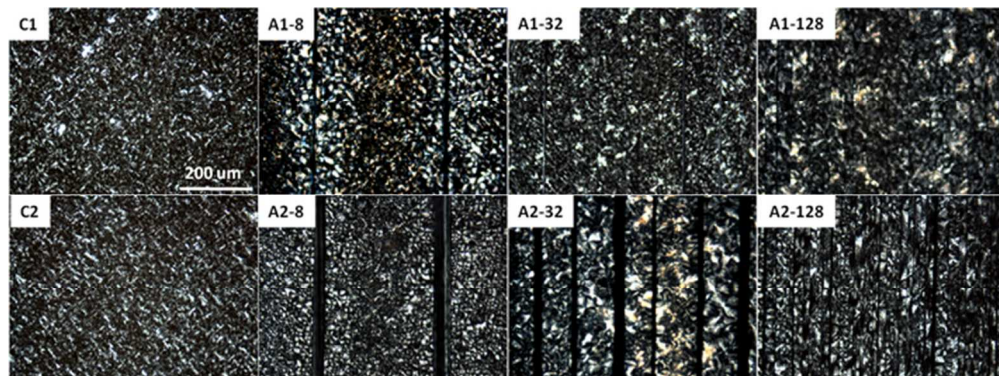


Fig. 4 Polarized optical micrographs of the conventional and multilayered blends morphologies.  
60x22mm (300 x 300 DPI)

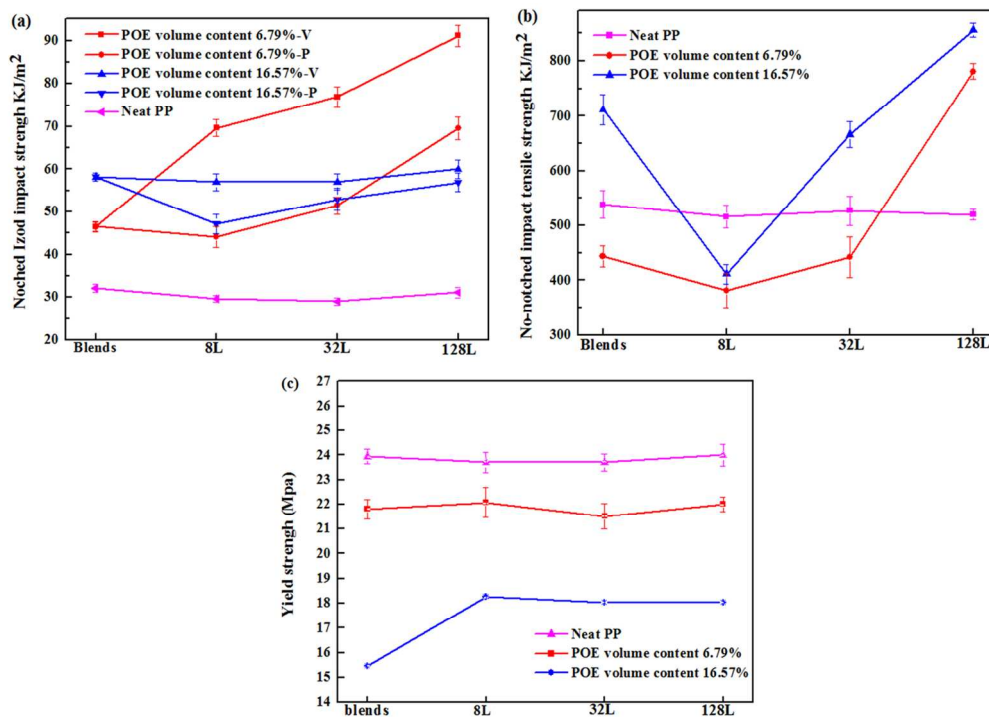


Fig. 5 Mechanical properties of the alternating multilayered, conventional blends and neat PP. (a): notched Izod impact strength though different directions; (b) no-notched impact tensile strength; (c): tensile yield strength.

80x57mm (600 x 600 DPI)

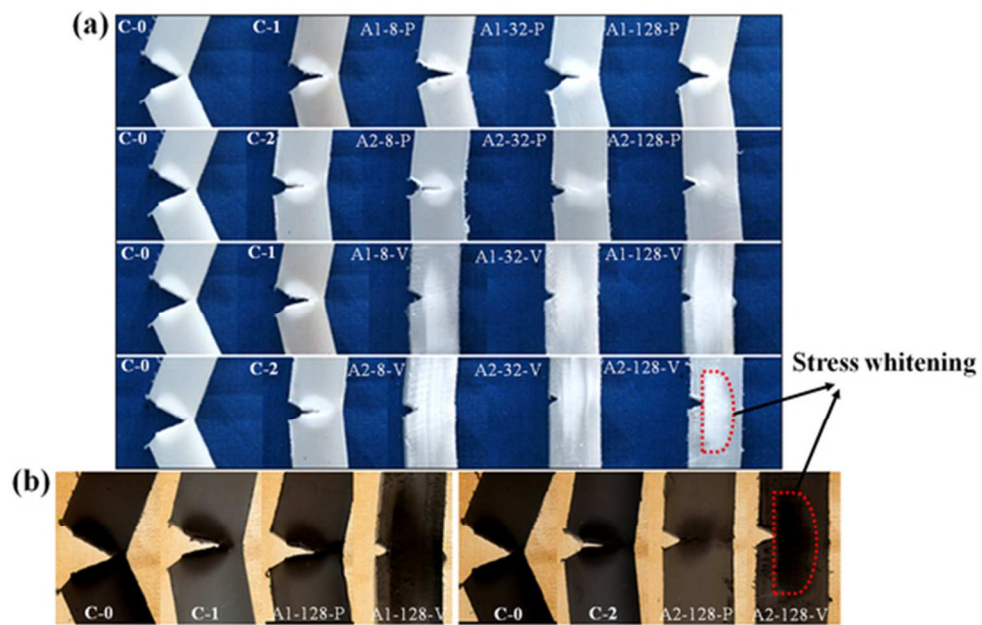


Fig. 6 Photographs of Izod samples taken after the notched impact test (a: normal photographs; b: typical photographs treated by the Image-Pro-Plus soft with the Invert Contrast Model)

51x32mm (300 x 300 DPI)

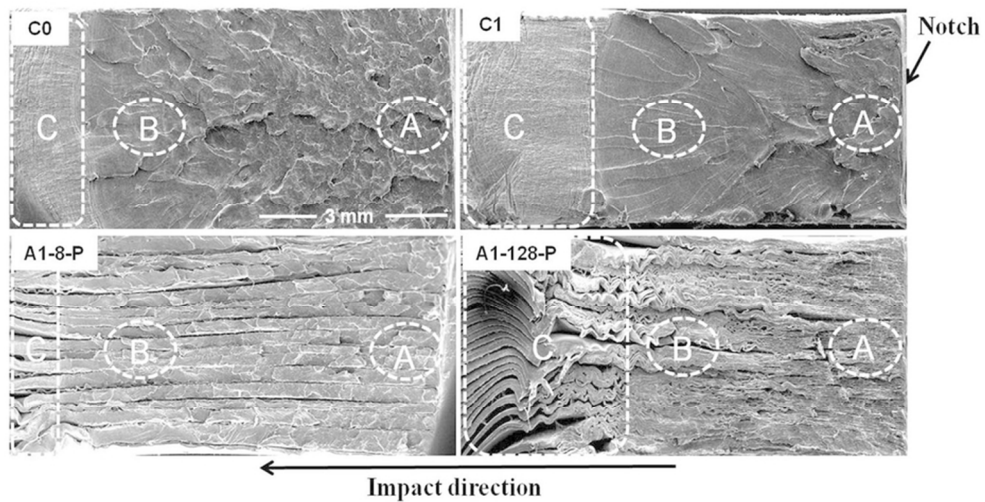


Fig. 7 SEM images of the impact fracture surface of neat PP (C0), conventional blend (C1) and the multilayered blends (A1-8-P and A2-128-P) at low magnification. A, B indicates the crack initiation zone, and crack propagation zone, respectively. The zone C marked by rectangular-shaped dashed line represents the unbroken part of the samples during the impact fracture process.  
80x40mm (300 x 300 DPI)

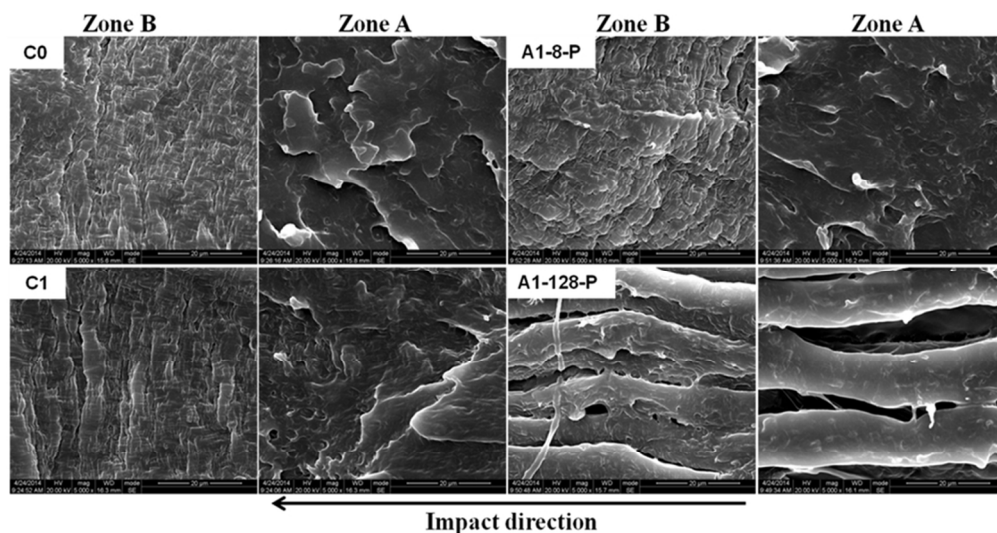


Fig. 8 SEM images of the impact fracture surface of neat PP (C0), conventional blend (C1) and the multilayered blends (A1-8-P and A2-128-P) at high magnification. The images were obtained from the different zones shown in Figure. 7. For the A1-8-P, the images were taken from the PP layers. The scale bars present 20  $\mu\text{m}$ .  
90x48mm (300 x 300 DPI)

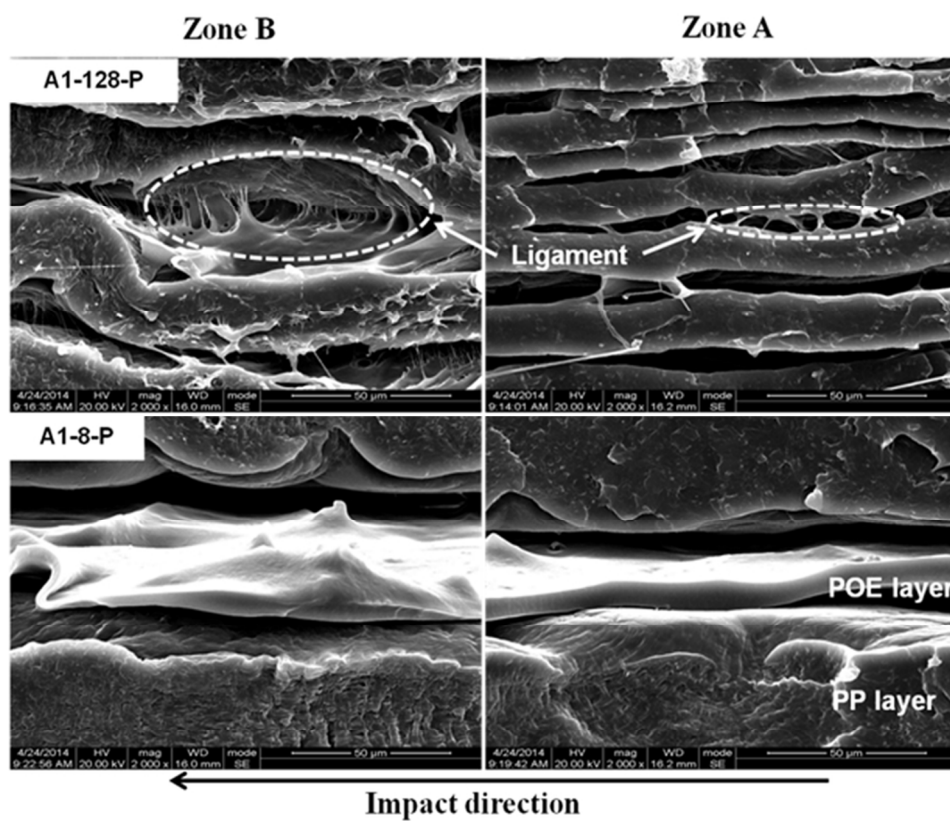


Fig. 9 SEM images of the interfaces delaminations from the impact fracture surface of the multilayered blends (A1-8-P and A2-128-P) at high magnification. The images were obtained from the different zones shown in Figure. 7. The scale bars present 50 μm.  
80x66mm (300 x 300 DPI)

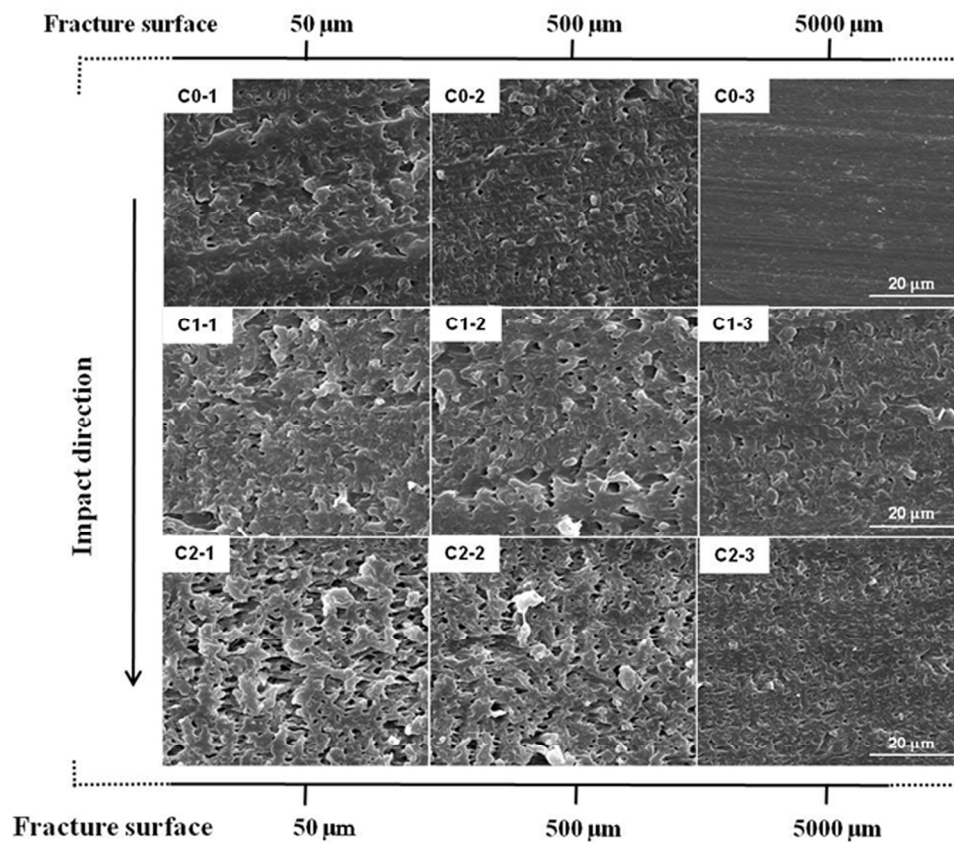


Fig. 10 SEM micrographs of the cross sections underneath the impact fracture surface of the neat PP (C0), conventional blends (C1 and C2) and multilayered blends (A1-128-V, A1-128-P, and A2-128-V, A2-128-P). The scale bars present 20 μm. The location, from where the micrographs were taken, are the zone under the impact fractured surface, 50 μm, 500 μm and 5000 μm away and labeled 1, 2 and 3, respectively.  
129x110mm (300 x 300 DPI)

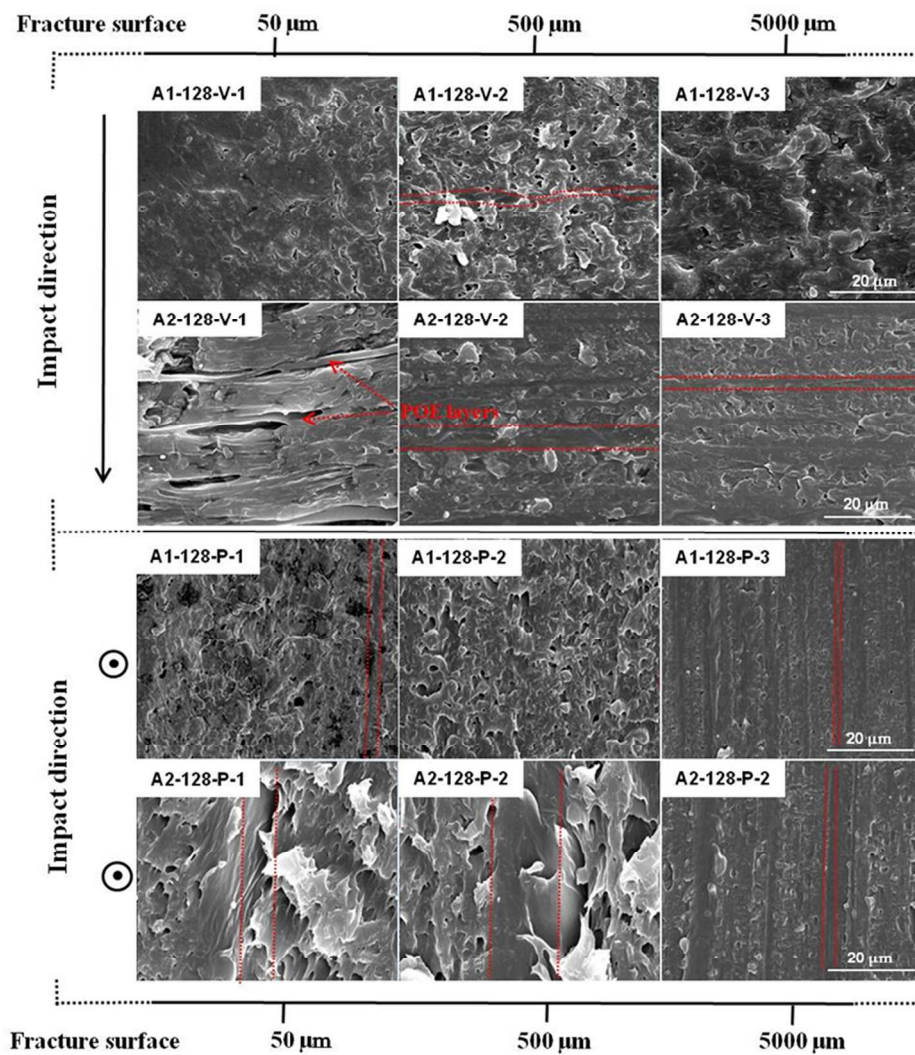


Fig. 10 Continued...  
119x127mm (300 x 300 DPI)

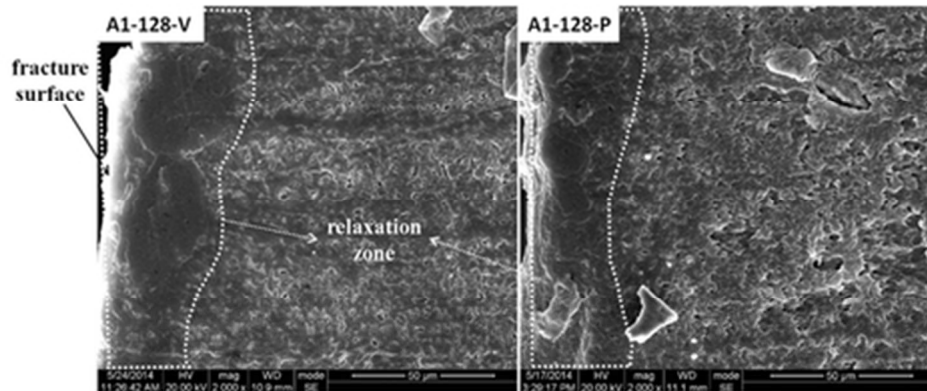


Fig. 11 SEM micrographs of the cross sections underneath the impact fracture surfaces of the A1-128-V and the A1-128-P, the fracture surface locates at the left. The dashed zone presents the relaxation zone, which formed during the impact process.  
39x16mm (300 x 300 DPI)

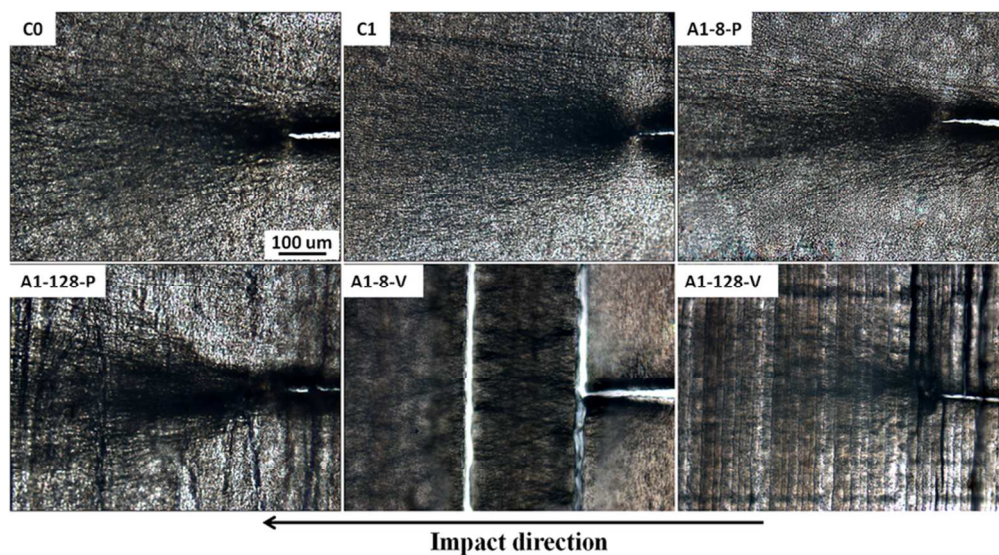


Fig. 12 Craze initiation patterns of the samples after the Izod notched part-impact test. (C0: neat PP; C1: conventional blend; A1-8-P and A1-128-P: multilayered blends impacted paralleled to the layer plane; A1-8-V and A1-128-V: multilayered blends impacted vertical to the layer plane)  
80x44mm (300 x 300 DPI)

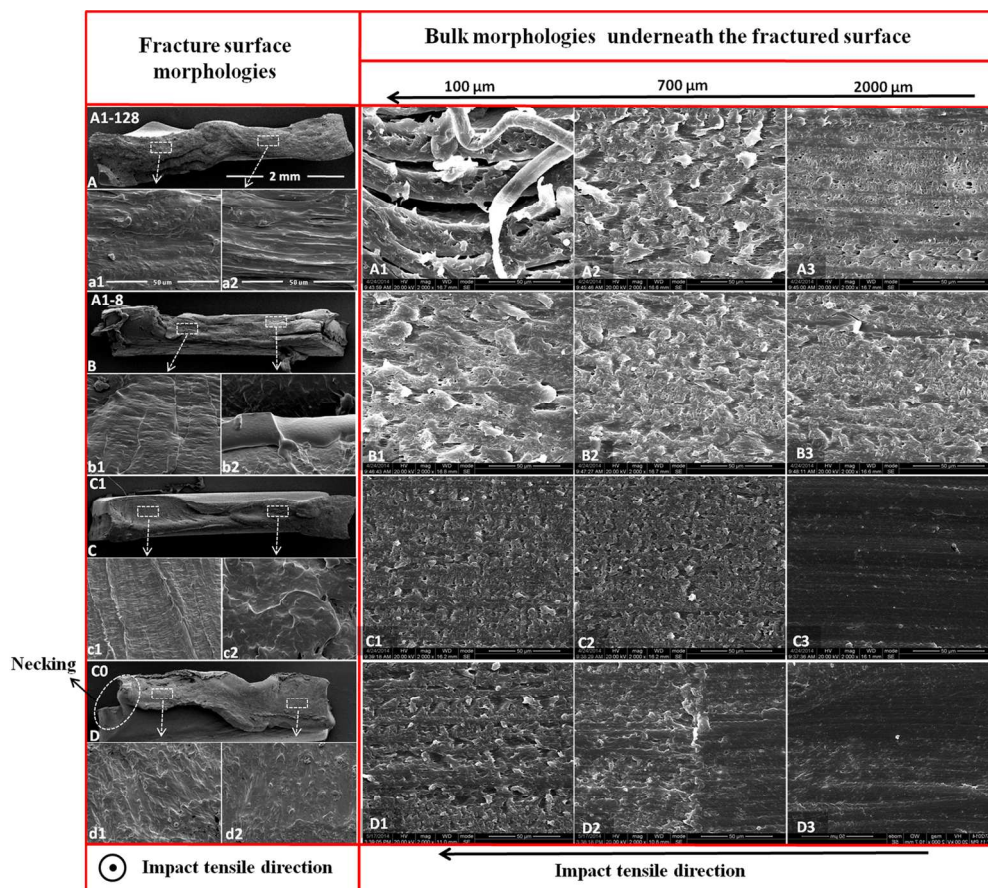


Fig. 13 SEM images of the no-notched impact tensile fracture surface morphologies and the bulk morphologies beneath the fracture surface of the multilayered blends (A1-8 and A1-128), conventional blend (C1) and the neat PP (C0) at different magnification. For the low and high magnification, the scale bars present 2 mm and 50 μm, respectively. The subscript 1, 2 and 3 of the A1~D3 presents 100 μm, 700 μm and 2000 μm away from the fracture surface, respectively.  
141x124mm (300 x 300 DPI)

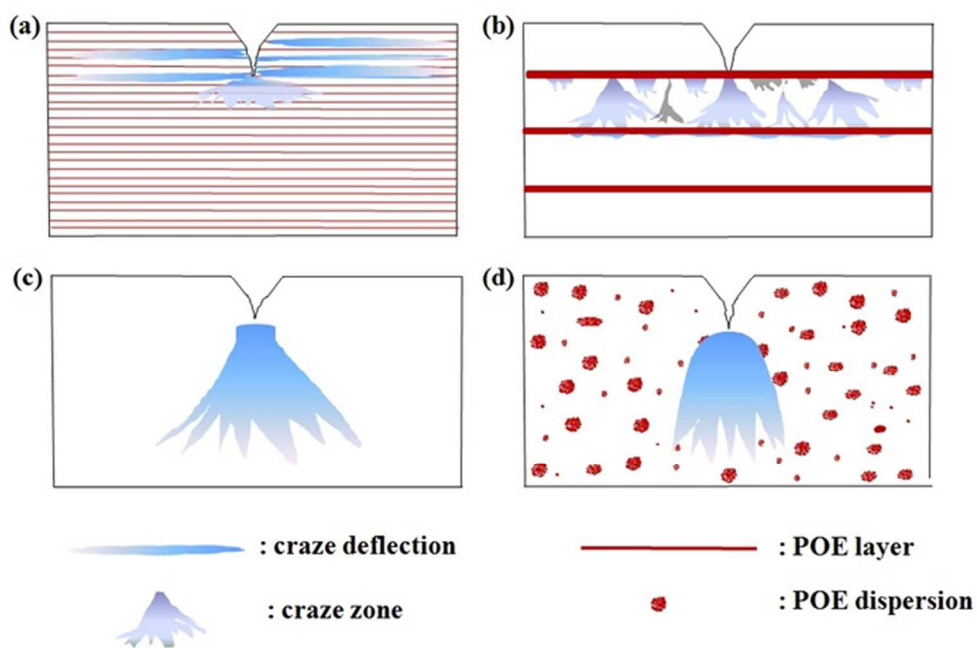


Fig. 14 Schematic for the craze patterns of the typical multilayered and conventional blends during the part-impact test. (a): A1-128-V; (b): A1-8-V; (c): A1-128-P; (d):C1.  
59x39mm (600 x 600 DPI)

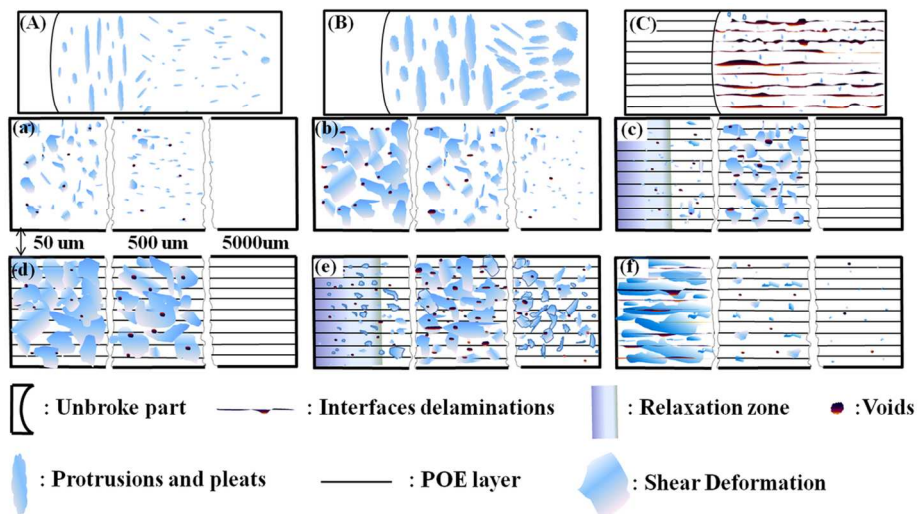


Fig. 15 Schematic illustrations for the fracture surface morphologies and the bulk morphologies beneath the fracture surface. A~B present the fracture surface of C0, C1 and A1-128-P, respectively. a~f present the bulk morphologies beneath the fracture surface 50μm, 500μm and 5000μm away. ((A), (a): C0; (B), (b): C1; (C), (c): A1-128-P; (d): A2-128-P; (e): A1-128-V and (f): A2-128-V)  
59x30mm (600 x 600 DPI)